IOP Publishing and International Atomic Energy Agency Nuclear Fusion
Nucl. Fusion **47** (2007) 1376–1382 doi:10.1088/0029-5515/47/9/040

Progress towards steady state at low aspect ratio on the National Spherical Torus Experiment (NSTX)

D.A. Gates[1], J. Menard[1], R. Maingi[2], S. Kaye[1], S.A. Sabbagh[3], S. Diem[1], J.R. Wilson[1], M.G. Bell[1], R.E. Bell[1], J. Ferron[4], E.D. Fredrickson[1], C.E. Kessel[1], B.P. LeBlanc[1], F. Levinton[5], J. Manickam[1], D. Mueller[1], R. Raman[6], T. Stevenson[1], D. Stutman[7], G. Taylor[1], K. Tritz[7], H. Yu[5] and the NSTX Research Team

[1] Princeton Plasma Physics Laboratory, Princeton University, Princeton, NJ, USA
[2] Oak Ridge National Laboratory, Oak Ridge, TN, USA
[3] Department of Applied Physics, Columbia University, NYC, NY, USA
[4] General Atomics, San Diego, CA, USA
[5] Nova Photonics, Princeton, NJ, USA
[6] University of Washington, Seattle, WA, USA
[7] Johns Hopkins University, Baltimore, MD, USA

Received 9 January 2007, accepted for publication 31 July 2007
Published 3 September 2007
Online at stacks.iop.org/NF/47/1376

Abstract
Modifications to the plasma control capabilities and poloidal field coils of the National Spherical Torus Experiment (NSTX) have enabled a significant enhancement in shaping capability which has led to the transient achievement of a record shape factor ($S \equiv q_{95}(I_p/aB_t)$) of ~41 (MA m^{-1} T^{-1}) simultaneous with a record plasma elongation of $\kappa \equiv b/a \sim 3$. This result was obtained using isoflux control and real-time equilibrium reconstruction. Achieving high shape factor together with tolerable divertor loading is an important result for future ST burning plasma experiments as exemplified by studies for future ST reactor concepts, as well as neutron producing devices, which rely on achieving high shape factors in order to achieve steady state operation while maintaining MHD stability. Statistical evidence is presented which demonstrates the expected correlation between increased shaping and improved plasma performance. Plasmas with high shape factor have been sustained for pulse lengths which correspond to $\tau_{pulse} = 1.6s \sim 50\tau_E \sim 5\tau_{CR}$, where τ_{CR} is the current relaxation time and τ_E is the energy confinement time. Plasmas with higher $\beta_t \sim 20\%$ have been sustained for $\tau_{pulse} = 1.2s \sim 25\tau_E \sim 3\tau_{CR}$ with non-inductive current fractions $f_{NI} \sim 50\%$, with ~40% pressure driven current and ~10% neutral beam driven current. An interesting feature of these discharges is the observation that the central value of the safety factor $q(0)$ remains elevated and constant for several current diffusion times without sawteeth, similar to the 'hybrid mode'. Calculations of the profiles of inductive and non-inductive current are compared with measurements of the total current profile and are shown to be in quantitative agreement. Results are shown from experiments which investigate the applicability of high harmonic fast waves (HHFWs) and electron Bernstein waves (EBWs) as current drive and heating sources, and the possibility of LHCD for future ST devices is raised. A calculated scenario which provides 100% non-inductive current drive is described. NSTX operates with peak divertor heat fluxes which are in the same range as those expected for the ITER device, i.e. with $P_{heat_{max}} \sim 10\,MW\,m^{-2}$. High triangularity, high elongation plasmas on NSTX have been demonstrated to have reduced peak heat flux to the divertor plates to $<3\,MW\,m^{-2}$.

PACS numbers: 52.55.Fa, 52.55.Dy, 52.55.Rk

(Some figures in this article are in colour only in the electronic version)

1. Introduction

The spherical torus (ST) concept [1] has been proposed as a potential fusion reactor [2] as well as a component test facility (CTF) [3] due to its relatively low capital cost and more attractive maintenance schemes. The National Spherical Torus Experiment (NSTX) was designed [4] to develop the understanding of the fundamental physics issues which need to be addressed before these forward looking designs can be realized. In particular, one of the fundamental differences between low aspect ratio and standard aspect ratio tokamaks is the relatively small space available in the central conductor for a neutron shield at low aspect ratio. In order to provide sufficient shielding to incorporate superconducting toroidal field (TF) magnets, standard aspect ratio tokamaks employ a neutron shield of order 1 m in thickness. This is required to reduce the nuclear heating of the superconducting coil to acceptable values. The central conductor of low aspect ratio devices typically have radii less than 1 m. For this reason, the TF conductor in an ST burning plasma device is usually imagined to be made of normally conducting material. Minimization of the recirculating power from this normally conducting TF coil in turn determines the minimum allowable ratio of plasma pressure to toroidal field energy $\beta_t \equiv 2\mu_0\langle P\rangle/B_t^2$ where $\langle P\rangle$ is the volume averaged pressure and B_t is the TF at the plasma geometric centre.

Additionally, it is very difficult to envision a multi-turn transformer coil that can survive in this high neutron flux environment. In addition to the obvious need for a plasma startup scheme (e.g. NSTX is investigating coaxial helicity injection [5] as a potential initiation mechanism), it is paramount to maximize the bootstrap current and to incorporate efficient non-inductive current drive schemes at low aspect ratio, so as to reduce the external current drive power requirements. Optimizing the bootstrap current forces operation at high values of the ratio of plasma pressure to poloidal magnetic field $\beta_p \equiv 2\mu_0\langle P\rangle/\langle B_p\rangle^2$ where $\langle P\rangle$ is the volume averaged pressure and $\langle B_p\rangle$ is the average poloidal field in the plasma, since $f_{bs} \sim \sqrt{\epsilon}\beta_p$, where f_{bs} is the bootstrap fraction, $\epsilon \equiv 1/A \equiv a/R$, with a and R the plasma minor and major radii, respectively.

Since the maximum pressure in the plasma is determined by the Troyon-limit given by $\beta_N < C_T$ where $\beta_N \equiv \beta_t a B_t/I_p$ with I_p the plasma current, the simultaneous requirements of high β_p and high β_t are at odds with each other. Raising the plasma current serves to raise the attainable β_t, but simultaneously reduces β_p (by increasing the $\langle B_p\rangle$). This conflict is the motivation for attaining high plasma shaping in toroidal confinement devices. It allows for the improvement of both parameters of interest in a steady state tokamak, β_t and f_{bs}. It also motivates the definition of a performance parameter $f_{bs}\beta_t \sim S\beta_N^2$ [6] where $S \equiv q_{95}(I_p/aB_t)$ is the plasma shaping factor. We refer to the parameter $f_{bs}\beta_t$ as the sustainable β, β_{sus}.

2. Improvements in plasma shaping capability on NSTX

In 2002, a long term plan was developed for NSTX that would allow access to highly shaped plasmas [8]. The plan had three major components: (1) improved control system response time to permit better control of the $n = 0$, $m = 1$ vertical instability, (2) modification of the poloidal field coils to allow access to high triangularity simultaneously with high elongation and (3) improved real-time shape reconstruction to enable accurate control of these larger plasmas. The steps taken to achieve these goals are summarized below.

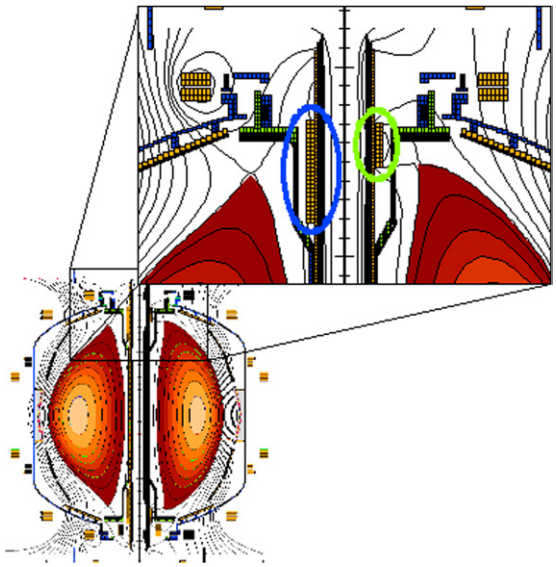

Figure 1. Detail view of the change made to the PF1A coil. The old coil is shown circled on the left, the new coil on the right.

The ability to make plasmas with high elongation ($\kappa \sim 2.5$) was shown on NSTX in 2004 [9, 10]. The means by which this goal was achieved was by a reduction in control system latency. NSTX uses a centralized all-digital CPU based control system. The technical details of the reduction in control system latency are discussed in [11].

Stability calculations made at the time of the long term planning exercise indicated that much stronger shaping was advantageous on NSTX and achievable by increasing the triangularity in concert with the elongation. Triangularity has a much stronger effect on the shape factor, S, at low aspect ratio than it does at high aspect ratio [12]. In order to achieve the desired improvements in machine shaping capability, modifications were made to the poloidal field coils on NSTX. In particular, the PF1A shaping coil shown in figure 1 was reduced in height, while roughly preserving its total current capability, to allow for the simultaneous achievement of high elongation and high triangularity. Predicted equilibria using this modified coil are shown in [10].

Along with the poloidal field coil modifications, the NSTX plasma control system [13] is upgraded [11] to support the expanded requirements for plasma shape control. In particular, precise rtEFIT/isoflux [14, 15] control of the plasma boundary during the current ramp-up phase at high elongation required the real-time acquisition of additional magnetic field sensors in the divertor region and a more accurate vessel current model [16] with additional measurements. Although not the subject of this paper, the control system data acquisition was also expanded to include capabilities for resistive wall mode feedback experiments [17] and error field control experiments [18] as described in [11].

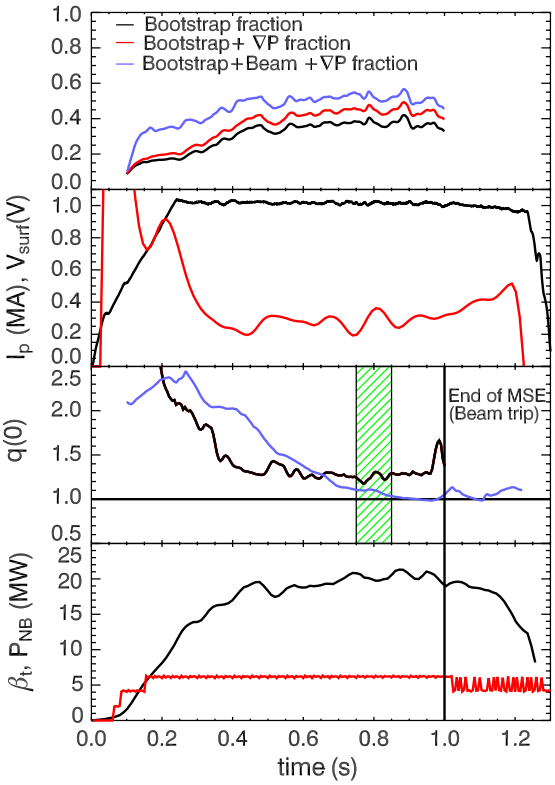

Figure 2. The time history of shot 120001 showing (*a*) the components of non-inductive current as indicated in the plot legend, (*b*) the plasma current (black) and the surface voltage (red), (*c*) the reconstructed $q(0)$ (black) and $q(0)$ as determined by a TRANSP magnetic diffusion calculation (blue) and (*c*) β_t (black) and the neutral beam power (red). The profiles in figure 6 are calculated over time interval indicated in green.

Whereas the expanded technical capabilities were in place at the end of 2005, the first NSTX run that took full advantage of these capabilities was in 2006. Optimization of the run scenarios developed in 2005 have led to a 25% increase in pulse length. These recent results are described below.

3. Shape control and global performance

During the 2006 campaign, the target equilibrium identified during the design process for the specified upgrades was achieved and maintained at $I_p = 1$ MA with a 1 s flat-top. The time history of an example shot with strong shaping ($\kappa(\equiv b/a) \sim 2.4$, $\delta \sim 0.8$) is shown in figure 2. The calculated fraction of non-inductive current in this discharge is ~50%. Analysis of the components of the current profile for this discharge are discussed in section 5.

Additional experiments have led to the achievement of a record value of the plasma shaping parameter $S \equiv q_{95} I_p/(aB_t) = 41$, simultaneously with the achievement of record elongation, $\kappa = 3$. The previous record controlled value of plasma elongation, $\kappa \sim 2.8$ was achieved on TCV [19]. It should be noted that the high elongation achieved on TCV was a much more impressive technical effort than the higher elongation achieved on NSTX. Low aspect ratio has higher natural elongation, which has been pointed out as an advantage of the ST [1]. The maintenance of the current profile so that low values of l_i are maintained is crucial for achieving high κ as shown in [10]. Higher values of elongation have been reported in transient plasmas on the START device [20], but these were uncontrolled. For the discharge in figure 3, $\kappa > 2.8$ for 40 ms which is $\sim 3\tau_{vert}$, where τ_{vert} is the growth time for the $n = 0, m = 1$ (vertical) plasma mode. A flux plot of the record κ equilibrium is shown in figure 3.

The predicted improvement in performance as a function of increased plasma shaping is confirmed in figure 4. Each point in this figure represents the value of β_t time averaged over the I_p flat-top plotted versus the flat-top time. The data are sorted in two different ways: in the lower frame by shape factor, S, and in the upper frame by year. As can be seen from the figure, the increasing shape factor on NSTX has led to an increase in both the maximum pulse length and the average value of β_t. For example, for $S < 20$ the maximum pulse length was $\tau_{pulse} = 0.6$ s and the maximum $\beta_t \sim 12\%$, whereas for $S > 30$ the maximum pulse length was $\tau_{pulse} = 1.0$ s and the maximum $\beta_t \sim 20\%$. The shapes of the upper boundaries in this plot are a direct result of the relationship $f_{bs}\beta_t \sim S\beta_N^2$. For a given S, the upper bound of the operating space is determined by $\beta_n = \beta_{N(max)}$, so for higher β_t one has lower f_{bs} yielding a shorter pulse. Increasing S acts as a multiplier on this curve. This is true in any device, such as NSTX, wherein the available transformer flux limits the pulse length (as is eventually the case for all devices that employ ohmic current drive).

4. MHD analysis high of elongation discharges

To date, the highest performance has not been achieved at the highest values of elongation. The reason for this lies in the method by which the plasma elongation was raised. The elongation of the NSTX vacuum vessel is ≈2.5. Therefore, in order to raise κ beyond this value it is necessary to shrink the minor radius. The method that was used to achieve the reduction in minor radius in the discharge shown in figure 3 was to increase the distance between the plasma and the outer vacuum vessel (i.e. increase the outer plasma wall gap). This has the effect of moving the plasma away from the copper stabilizing plates on the outboard wall. When this was done, it was observed that the maximum achievable β_N was reduced to $\beta_N \approx 3.5$, similar to the value that is expected for the no-wall β-limit on NSTX. It was therefore hypothesized that the cause for the reduction in $\beta_{N_{max}}$ was due to the loss of wall stabilization. To verify this effect we have utilized the PEST [21] stability code to calculate the MHD stability of this high elongation discharge.

The results are shown in figure 5. The figure shows the no-wall growth rate of the most unstable eigenmode, which has an external kink like character, plotted along with the time history of the normalized β_N. The figure illustrates several points. Firstly, the maximum $\beta_N \approx 3.5$ whereas a more typical value for beam-heated NSTX discharges is $\beta_{N_{max}} \approx 6$. Secondly, the pressure collapses twice in the discharge with the collapses corresponding to the onset of MHD instability. Thirdly, since these are modes that are only present in the no-wall limit, we can conclude that the wall is no longer stabilizing these instabilities.

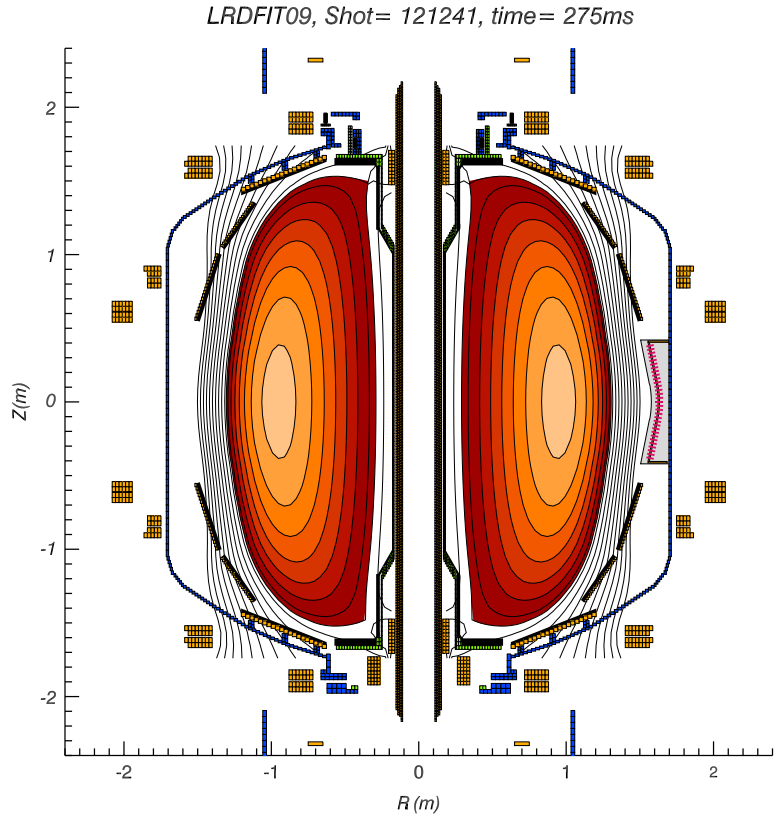

Figure 3. Flux plot of the record elongation ($\kappa = 3$) plasma equilibrium.

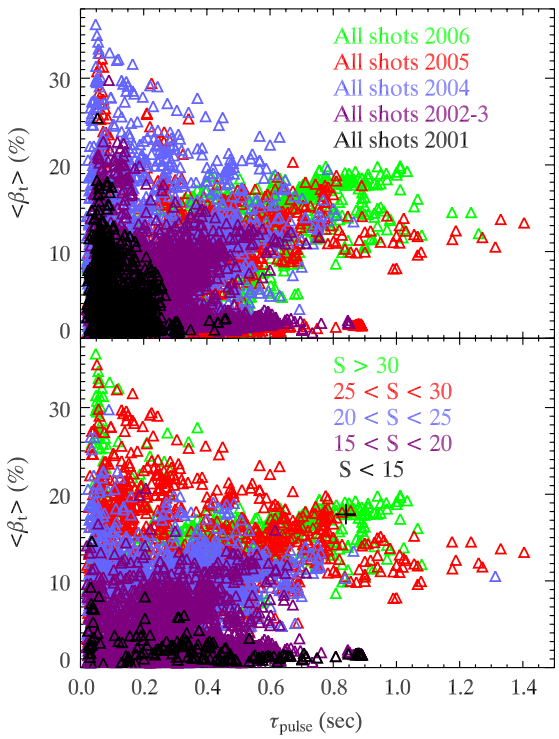

Figure 4. β_t averaged over the plasma current flat-top for each shot in the NSTX database plotted versus the current flat-top time. The data is sorted according to year in the upper frame, and according to shape factor S in the lower frame.

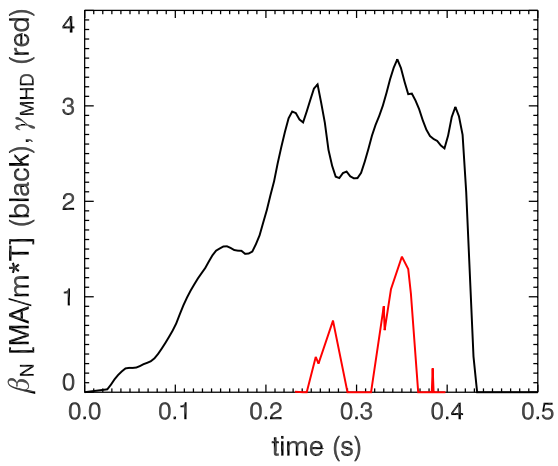

Figure 5. This figure shows the time history of β_N versus time for shot 121241 which had a record elongation (the plasma cross-section is shown in figure 3). Shown in red in the figure is the growth rate (in arbitrary units) of the $n = 1$ no-wall external kink as calculated by the PEST stability code. Note the good temporal correlation between the onset of instability and the collapse in β_N.

Given this information, it is reasonable to investigate whether shifting the plasma outwards (i.e. increasing the inner gap rather than increasing the outergap as was done for these discharges) will allow access to higher β-limits. This experiment will be attempted in the 2007 run campaign. Discussion of the future target equilibria follows in section 8.

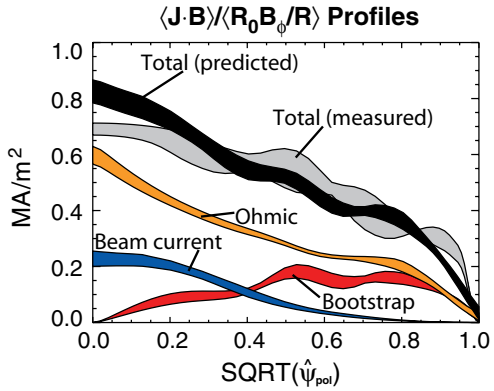

Figure 6. Components of the total current profile plotted versus flux label for shot 120001. The bootstrap current is in red, the ohmic current is in orange, and the beam driven current is in blue. The bands are variations during the time window for the calculation. The black trace is the total predicted current, and the grey is the total current as determined by equilibrium reconstruction with MSE.

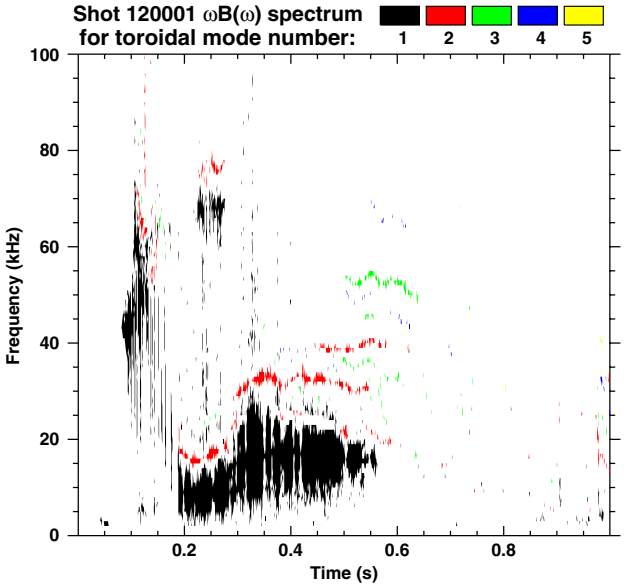

Figure 7. A spectrogram of magnetic fluctuations as measured by a Mirnov coil for shot 120001. The colours represent toroidal mode numbers as indicated in the legend. Notice the period of time after 0.6 s where there are only small amplitude high-n MHD modes present.

5. Current profile analysis

It is important to demonstrate the utility of models which are routinely used to calculate the magnitude and the profiles of non-inductive current. This establishes the confidence with which one can make quantitative predictions regarding the performance of future devices. It also verifies the applicability of these models at low aspect ratio, expanding the parameter space over which the models have been bench-marked against experiment. In order to make a valid comparison with data, an accurate measurement of the plasmas internal field distribution is required. The motional Stark effect diagnostic on NSTX, which measures the magnetic field pitch angle at 12 spatial locations, is the only such measurement currently available for any ST. This capability has been used to make a quantitative comparison between the measured and expected plasma current profiles using a method first described in [22].

Shown in figure 6 are the total plasma current profile as determined by the MSE measurement and reconstructed by the EFIT [23] equilibrium reconstruction code. Also plotted in the figure is (1) the neutral beam driven current as calculated by the TRANSP code [24], (2) the neoclassical pressure driven currents according to a recent calculation that includes corrections important at low aspect ratio [25] and (3) the inductively driven current calculated according to the inferred time varying toroidal electric field as calculated by taking the time derivative of the flux from the equilibrium reconstructions multiplied by the calculated neoclassical resistivity. The neoclassical resistivity is also taken from [25]. The magnitude of the low aspect ratio corrections from [25], which come from using the local trapped particle fractions instead of aspect ratio scaling terms for the collisionality corrections, are typically of order 10–20%.

The reconstruction process and data analysis that goes into this detailed profile comparison are described in detail in [26]. All parameters in the predicted profiles are measured (n_e, T_e, (from Thomson scattering) T_i, n_i, Z_{eff}, (from charge exchange recombination spectroscopy, since carbon is the dominant impurity species on NSTX) and $J_\parallel$ (from motional Stark effect polarimetry and external magnetics)) except the fast ion pressure profile which is calculated according to classical slowing down theory in TRANSP. This particular discharge has a non-inductive current fraction of $f_{NI} \sim 50\%$, less than the maximum values of $f_{NI} \sim 65\%$ reported previously in [7], but has higher $\beta_t \sim 20\%$ similar to the values typical for ST-CTF designs. The pressure driven current fraction is $f_{pres} \sim 40\%$ (including the diamagnetic and Pfirsch–Schluter currents), also very close to values required for a CTF (typically ~50%). This discharge has $f_{bs}\beta_t \sim 7\%$, which is a record value. In an ST-CTF, the neutral beam driven current fraction $f_{NBI} \sim 50\%$ is expected to be much higher, due to the expected lower collisionality at higher B_t (see [3] for a discussion of NBI current drive efficiency). The profile of the total parallel current inferred from MSE measurements shown in figure 6 should be compared directly with the sum of the predicted parallel currents. The agreement between predicted and measured values is quite good with a maximum discrepancy of ~10%. The profiles do vary somewhat in the core of the discharge. The central safety factor, which is shown in figure 2 stays elevated for $\sim 2\tau_{CR}$ [27], similar to the 'hybrid mode' proposed for ITER. For this discharge however, there is no clear evidence of a large scale low frequency MHD instability to drive fast particle diffusion. The only measured MHD modes have relatively high toroidal mode numbers $n = 3$–5 during most of the period of elevated central q. A spectrogram of the measured magnetic fluctuations for the same plasma discharge presented in figure 2 is shown in figure 7. One possible explanation is the large number of high frequency compressional and global Alfven instabilities that are observed in many NSTX discharges with neutral beam heating [29]. Work is ongoing into what is responsible for the maintenance of the elevated central safety factor. The clear advantage of this

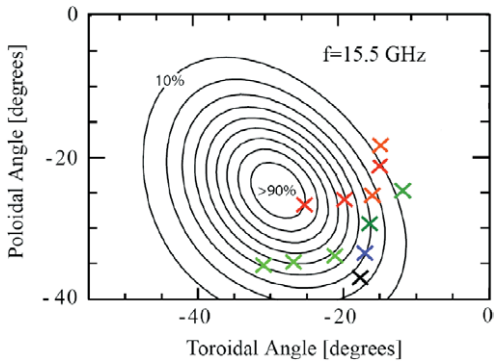

Figure 8. Data on efficiency of EBW emission from identical plasmas for which the EBW antenna pointing angle is varied. The colours represent efficiencies of 81–90% (red), 71–80% (orange), 61–70% (green), 51–60% (blue), 31–40% (black). The ellipses are contours of theoretically predicted emission efficiency.

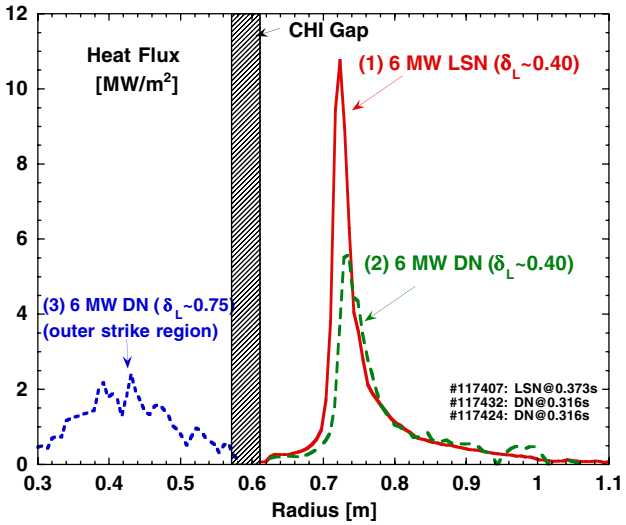

Figure 9. The peak heat flux versus major radius for three divertor configurations: (1) low δ lower single null, (2) low δ double null and (3) high δ double null. All three configurations had identical heating power. The peak heat flux reduces by a factor of ∼5.

regime of operation, which has a confinement enhancement factor of $H89P \sim 2$, is that the observed mode activity does not degrade confinement.

6. RF heating and current drive

Spherical tokamaks typically operate in a very different regime than standard aspect ratio tokamaks, in that the spherical tokamak plasma is typically overdense. This is the direct result of the low axial magnetic field in an ST lowering the cyclotron frequency so that it is well below the plasma frequency. This means the electromagnetic waves that are used to drive current at standard aspect ratio are cut-off in an ST. For this reason, electrostatic plasma waves are of interest for current drive in STs.

The EBW is especially attractive since it has been shown theoretically to have very high efficiency Ohkawa type current drive. Research into the coupling of the EBW out of the plasma has indicated that the O–X–B mode conversion scheme can have efficiencies as high as 80–90%. This is encouraging, since the EBW is an electrostatic wave that is evanescent in the plasma boundary, an efficient mode coupling scheme is required in order to launch high power electromagnetic waves that can transfer their energy to the plasma. Results of an experiment to investigate the angular variation of the emission efficiency are shown in figure 8 and show good agreement with theoretical predictions. This experiment is described in more detail in [30]. The good coupling results to date have been observed in the L-mode, with much lower efficiencies of ∼30% in the H-mode.

Research into the use of HHFW heating on NSTX has for the first time yielded high efficiency coupling using the current drive phasing ($k_{\|} = 7\,\mathrm{m}^{-1}$) of the NSTX HHFW antenna. The improved coupling was observed at higher values of TF $B_t = 0.55\,\mathrm{T}$. The higher field is thought to have reduced the parasitic coupling of the launched RF power to the parametric decay instability, which had been observed to interfere with the coupling at lower TF [28]. This is an important step towards using the HHFW as a tool for driving current during the startup phase of the NSTX plasma to aid plasma current ramp-up. The HHFW experiments are described in more detail in [18].

7. Divertor power loading

Controlling peak heat flux is a critical issue for ITER and other burning plasma experiments, including potential future ST experiments. An additional benefit of strong shaping, and in particular high triangularity, at low aspect ratio is strong divertor flux expansion of the outboard seperatrix. In lower flux-expansion regimes, the divertor power loading on NSTX is similar to that expected for ITER as first shown in [31]. Figure 9 shows the effect of varying plasma shape on divertor power loading. Each shot in the figure has identical heating power, but by changing from low triangularity $\delta \sim 0.4$ single null to low triangularity double-null to high triangularity $\delta \sim 0.8$ double-null, the peak heat flux is successively reduced from $\sim 10\,\mathrm{MW\,m^{-2}}$ to $\sim 5\,\mathrm{MW\,m^{-2}}$ to $\sim 2.5\,\mathrm{MW\,m^{-2}}$. The ability to study heat flows in varying divertor geometries is a powerful tool for understanding the impact of high heat flux on plasma facing materials. In addition, the ability to raise the divertor power load to ITER-like levels in NSTX provides an excellent opportunity to qualify differing divertor technologies in a smaller, and hence less costly environment. An additional benefit of the high δ double-null configuration is that it is consistent with operating in a small-ELM regime, first described in [32].

8. Projections to 100% non-inductive current drive

Using the current drive prediction methods described in section 5, self-consistent scenarios have been identified by which NSTX can attain 100% non-inductive current drive using only bootstrap current and neutral beam current drive. The profiles of non-inductive current for one such scenario are shown in figure 10. The bulk of the current in this case is bootstrap current, and the plasma has high $\beta_p \sim 2.7$. The

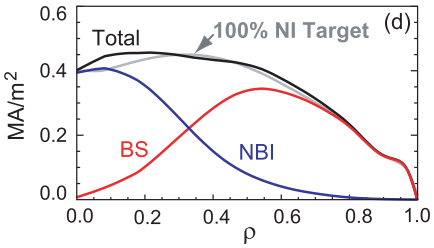

Figure 10. Calculated current profiles for a 100% non-inductively driven scenario predicted for NSTX. Successful realization of this scenario depends on reducing collisionality.

required shaping for this scenario, $\kappa \sim 2.6$, $\delta \sim 0.8$ has already been achieved. However, in order to achieve the goal of 100% non-inductive operation, it will first be necessary to raise the electron temperature and also lower the electron density beyond that which has been typically achieved, in order to reduce the collisionality. The required increase in electron temperature is on the order of 50% for the scenario described in figure 10. Reduction in collisionality affects not only the neutral beam driven current but also the bootstrap current in the regime that NSTX currently operates. The regime of operation that is required to achieve full non-inductive current drive in NSTX is different than that anticipated on a CTF-like device due to the lower electron temperatures achievable at the NSTX TF. For a CTF-like device, it is anticipated that the lower collisionality will make NBICD much more efficient, and that 100% non-inductive operation will be achievable with 50% NBICD and 50% bootstrap fraction.

9. Summary and conclusions

NSTX has demonstrated significant progress in plasma shape control capability as evidenced by the simultaneous achievement of record plasma shaping factor $S = 41\,(\mathrm{MA\,m^{-1}\,T^{-1}})$ and $\kappa = 3$. These goals were achieved as a result of machine and control system improvements that have taken place over the last three years. The improved shaping capability has broadened the NSTX operating space to include plasmas with $f_{\mathrm{NI}} \sim 50\%$ simultaneous with $\beta_{\mathrm{t}} \sim 20\%$. MHD analysis of these highly shaped plasmas indicates that future efforts should be directed at improving the coupling to the conducting structure to help stabilize the external kink instability. Theoretical predictions of the total current profile based on the actual measured kinetic profiles are in agreement to a level of ~10%, with the total measured current. This predictive capability gives increased confidence in the ability to project current drive requirements for future devices. Several promising RF current drive options are being investigated including HHFW, EBW and the possibility of LHCD in future devices. However, 100% non-inductive operational scenarios have been identified using NBICD and bootstrap current alone. Future work on NSTX will focus on reducing the electron collisionality via edge recycling control. These results are promising for the ST concept as a future CTF, and as a future fusion reactor.

Acknowledgment

This work was supported by the US Department of Energy Grant under contract number DE-AC02-76CH03073.

References

[1] Peng Y.-K.M. and Strickler D.J. 1986 *Nucl. Fusion* **26** 769
[2] Najmabadi F. and the ARIES Team 2003 *Fusion Eng. Des.* **65** 143
[3] Peng Y.-K.M. *et al* 2005 *Plasma Phys. Control. Fusion* **47** B263
[4] Ono M. *et al* 2000 *Nucl. Fusion* **40** 557
[5] Raman R., Jarboe T.R., Nelson B.A., Bell M.G. and Mueller D. 2007 *J. Fusion Energy* **26** 159
[6] Mau T.K. *et al* 1999 Physics basis for the ARIES-ST power plant *Proc. 18th IEEE/NPSS Symp. on Fusion Engineering (Albuquerque, NM)* pp 45–8 and http://ieeexplore.ieee.org/iel5/6866/18462/00849789.pdf
[7] Gates D.A. *et al* 2006 *Phys. Plasmas* **13** 056122
[8] Kessel C.E. *et al* 2005 *Nucl. Fusion* **45** 814
[9] Kaye S. *et al* 2005 *Nucl. Fusion* **45** S168
[10] Gates D.A. *et al* 2006 *Nucl. Fusion* **46** S22
[11] Gates D.A. *et al* 2006 *Fusion Eng. Des.* **81** 1911
[12] Gates D.A. and the NSTX National Research Team 2003 *Phys. Plasmas* **10** 1659
[13] Gates D.A., Mueller D., Neumeyer C. and Ferron J.R. 2000 *IEEE Trans. Nucl. Sci.* **47** 222(I)
[14] Gates D.A. *et al* 2006 *Nucl. Fusion* **46** 17
[15] Ferron J.R., Walker M.L., Lao L.L., St John H.E., Humphreys D.A. and Leuer J.A. 1998 *Nucl. Fusion* **38** 1055
[16] Gates D.A., Menard J.E. and Marsala R.J. 2004 *Rev. Sci. Instrum.* **75** 5090
[17] Sabbagh S.A. *et al* 2006 *Phys. Rev. Lett.* **97** 045004
[18] Menard J.E. *et al* 2007 Overview of recent physics results from the National Spherical Torus Experiment (NSTX) *Nucl. Fusion* **47** at press
[19] Hofmann F., Moret J.M. and Ward D.J. 1998 *Nucl. Fusion* **38** 1767
[20] Sykes A. 1994 *Plasma Phys. Control. Fusion* **36** B93
[21] Grimm R.C., Greene J.M. and Johnson J.L. 1976 *Methods in Computational Physics* vol 16, ed J. Killeen (New York: Academic) p 253
[22] Forest C.B. *et al* 1994 *Phys. Rev. Lett.* **73** 2444
[23] Lao L.L., St John H., Stambaugh R.D. and Pfeiffer W. 1985 *Nucl. Fusion* **25** 1421
[24] Hawryluk R.J. 1980 *Physics of Plasmas Close to Thermonuclear Conditions* vol 1 (Brussels: CEC) p 19
[25] Sauter O., Angioni C. and Lin-Liu Y.R. 1999 *Phys. Plasmas* **6** 2834
[26] Menard J.E. *et al* 2006 *Phys. Rev. Lett.* **97** 095002
[27] Mikkelsen D.R. 1989 *Phys. Fluids* B **1** 333
[28] Biewer T.M., Bell R.E., Diem S.J., Phillips C.K., Wilson J.R. and Ryan P.M. 2005 *Phys. Plasmas* **12** 056108
[29] Fredrickson E.D. *et al* 2001 *Phys. Rev. Lett.* **14** 145001
[30] Harvey R.W. *et al* 2006 *Proc. 21st Int. Conf. on Fusion Energy 2006 (Chengdu, China)* (Vienna: IAEA) CD-ROM file TH/P6-11 and http://www-naweb.iaea.org/napc/physics/FEC/FEC2006/html/index.htm
[31] Maingi R. *et al* 2003 *Nucl. Fusion* **43** 969
[32] Maingi R. *et al* 2005 *Nucl. Fusion* **45** 264